crystals

MDPI

Article

Enhanced X-ray Attenuating Efficiency of Silicon Dioxide Nanoparticles with Cesium Lead Bromide and 2,5-Diphenyloxazole Co-Embedded Therein

Geunpyo Choe †, Hyemin Kwon †, Ilhwan Ryu and Sanggyu Yim *

Department of Chemistry, Kookmin University, Seoul 02707, Korea; choigp@kookmin.ac.kr (G.C.); khm6434@kookmin.ac.kr (H.K.); ihryu@kookmin.ac.kr (I.R.)

* Correspondence: sgyim@kookmin.ac.kr

† These authors contributed equally to this work.

Abstract: An X-ray-attenuation-based in vivo imaging can be a promising candidate for real-time detection of cancer in an early stage due to its significantly longer penetration depth compared to currently investigated fluorescence-emission-based imaging techniques. It has recently been demonstrated that this novel concept of imaging is feasible using cesium lead bromide (CPB) quantum dots (QDs) stably embedded in silicon dioxide (SiO_2) nanoparticles (NPs). However, further improvements are necessary to realize its practical use, especially in terms of X-ray attenuation efficiency. In this study, we have found that the X-ray attenuation capability of CPB/SiO_2 NPs was significantly enhanced by embedding an organic X-ray scintillator, 2,5-diphenyloxazole (PPO), together with CPB QDs in the NPs. The embedment not only solved the water dispersibility and stability problem of PPO, but also significantly increased the Hounsfield unit of the NPs, which was proportional to the degree of X-ray attenuation, by 2.7 times.

Keywords: X-ray attenuation; attenuation-based imaging; cesium lead bromide; 2,5-diphenyloxazole; Hounsfield unit

Citation: Choe, G.; Kwon, H.; Ryu, I.; Yim, S. Enhanced X-ray Attenuating Efficiency of Silicon Dioxide Nanoparticles with Cesium Lead Bromide and 2,5-Diphenyloxazole Co-Embedded Therein. *Crystals* **2021**, *11*, 1531. https://doi.org/10.3390/cryst11121531

Academic Editor: Alessandro Vergara

Received: 9 November 2021
Accepted: 7 December 2021
Published: 8 December 2021

1. Introduction

Researches on the biological applications of semiconductor nanocrystals, such as in vivo imaging and diagnostics, have been steadily evolving [1,2]. Especially, emission-based optical imaging technologies using fluorescent nanomaterials have attracted attention in order to overcome the limited target-specificity and contrast issues of conventional tomographical techniques such as magnetic resonance imaging (MRI), computed tomography (CT), and positron emission tomography (PET) [3–5]. However, currently investigated fluorescence-emission-based approaches have a fatal drawback of short tissue penetration, that is, fluorophores existing deep inside the body are hardly detected outside [6–8]. Although fluorophores emitting the wavelength, λ, of longer tissue penetration, especially near-infrared-II (λ of 900–1700 nm), have extensively been investigated in recent years, they also have intrinsically limited penetration depth and a trade-off between the depth and the resolution [7,8]. To overcome the limitations of such emission-based imaging technologies, we have recently proposed an X-ray-attenuation-based imaging technique using cesium lead bromide (CPB; $CsPbBr_3$) quantum dot (QD)-embedded silicon dioxide (SiO_2) nanoparticles (NPs) that effectively attenuate incident X-rays [9]. Because X-rays have almost unlimited depth of tissue penetration, the X-ray-based imaging can be a plausible candidate for real-time in vivo detection of cancer wherever it is located in a body. When NPs, the surface of which is conjugated with cancer-specific antibodies, are injected intravenously into a tumor-grown mouse, a bright spot at the tumor position is clearly visible due to the target-specificity of the NPs and the outstanding X-ray attenuation capability of the CPB QDs therein.

However, there still remains much room for improving the X-ray attenuation quantum yield and stability of NPs for their practical use. Recently, it has been reported that the X-ray attenuating quantum efficiency of a CPB-containing liquid scintillator is significantly improved by adding organic scintillators such as 2,5-diphenyloxazole (PPO) [10]. In addition, the significantly short decay time (~7 ns) of PPO is also expected to result in a rapidly repeated consumption of incident X-ray photons [11,12]. The improvement was explained by the effective transfer of X-ray-induced charges from PPO molecules to CPB nanocrystals via the strong interaction between N atoms of PPO and Pb atoms of CPB. In the literature, a mixture of inorganic CPB nanocrystals and organic PPO molecules dispersed in octane is used as a liquid scintillator. However, it is not possible to use the mixture directly in vivo due to its extremely poor dispersibility and stability in water. In this study, we have solved both problems by encaging PPO molecules and CPB QDs simultaneously and stably in SiO_2 NPs. The synthesized CPB–PPO/SiO_2 NPs were highly dispersible in water and showed significantly improved the X-ray-attenuating efficiency, compared to the SiO_2 NPs containing CPB QDs only.

2. Materials and Methods

SiO_2 NPs containing CPB QDs and PPO molecules, denoted as CPB–PPO/SiO_2 NPs, were synthesized using a modified "rapid co-synthesis and double-encapsulation method", which was described elsewhere [9]. Briefly, 2 mL CPB precursor solution prepared by adding 0.3 g lead bromide (99.999%; Sigma-Aldrich, Seoul, Korea), 0.17 g cesium bromide (99.999%; Sigma-Aldrich, Seoul, Korea), 1.2 mL oleylamine (70%; Sigma-Aldrich, Seoul, Korea), 3.6 mL oleic acid (90%; Sigma-Aldrich, Seoul, Korea), and catalytic amount of ammonium hydroxide (28%; Deajung, Seoul, Korea) in 20 mL *N*,*N*-dimethylformamide (99.5%, Deajung, Seoul, Korea) were rapidly injected into a SiO_2 precursor solution containing 1600 µL tetramethyl orthosilicate (98%; Sigma-Aldrich, Seoul, Korea) and 200 mg PPO (grade for spectrometry; Sigma-Aldrich, Seoul, Korea) in 100 mL toluene (99.7%; Deajung, Seoul, Korea), followed by stirring at room temperature for 2 h. The synthesized CPB–PPO/SiO_2 NPs were collected using centrifugation and washed with ethanol three times, followed by annealing at 150 °C for 2 h to remove surface hydroxyl groups. For comparison, SiO_2 NPs containing CPB QDs only, denoted as CPB/SiO NPs, were also prepared in the same manner without the PPO in the above process.

The size and shape of the synthesized CPB/SiO_2 and CPB–PPO/SiO_2 NPs were characterized by field-emission scanning electron microscopy (FE-SEM, JSM-7610F; JEOL Ltd., Tokyo, Japan). The existence of the PPO molecules in the NPs was confirmed by a Fourier-transform infrared (FTIR) spectrometer (Nicolet™ iS™ 50 FTIR Spectrometer; Thermo Fisher, Waltham, MA, USA). The PPO leakage from the CPB–PPO/SiO_2 NPs was evaluated by electronic absorption measurements (Mega-800; Scinco, Seoul, Korea). Three milliliters of toluene were added into 3 mL of 1 mg/mL CPB–PPO/SiO_2 NP-dispersed aqueous solution. After vigorous stirring and phase separation, the toluene layer was taken, and the measurement was performed. The X-ray attenuation characteristics of the synthesized NPs were estimated by a micro-CT system (SKYSCAN 1176; Bruker, Billerica, MA, USA) at a tube potential of 50 kVp.

3. Results and Discussion

The basic strategy for synthesizing CPB–PPO/SiO_2 NPs is illustrated in Figure 1a. The embedment of individual CPB QDs without aggregation in SiO_2 NPs was successfully performed by the rapid co-synthesis of QDs and NPs, which was well presented in the earlier report [13]. Briefly, CPB/SiO_2 NPs were obtained by rapidly injecting a CPB precursor solution containing a catalyst for SiO_2 synthesis into a SiO_2 precursor solution, hence synthesizing CPB QDs and SiO_2 NPs simultaneously in a very short time. In this study, the additional embedment of PPO molecules with CPB QDs in SiO_2 NPs was successfully achieved by dissolving the PPO molecules in the SiO_2 precursor solution prior to the injection of the CPB precursor solution. The 512 nm-wavelength green emissions

of both the CPB/SiO_2 and CPB–PPO/SiO_2 NPs under UV irradiation indicated that the individual CPB QDs were well embedded inside the NPs since it was the typical emission of 4–15 nm CPB QDs (Figure 1b) [13,14]. As shown in the FE-SEM images (Figure 1c,d), the morphologies of the CPB/SiO_2 and CPB–PPO/SiO_2 NPs did not differ significantly, although the average particle size of the CPB–PPO/SiO_2 NPs was slightly larger than that of the CPB/SiO_2 NPs.

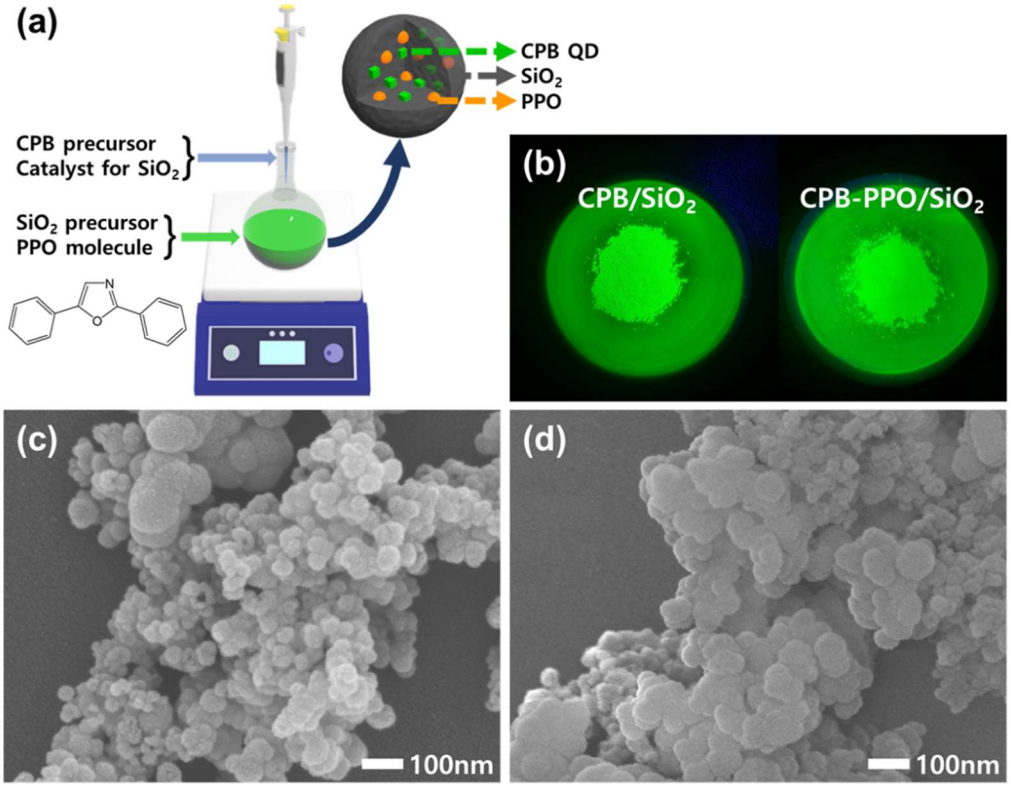

Figure 1. (**a**) A schematic illustration for the synthesis and structure of cesium lead bromide (CPB)–2,5-diphenyloxazole (PPO)/SiO_2 nanoparticles (NPs). (**b**) Photographs of CPB/SiO_2 and CPB–PPO/SiO_2 NPs taken under UV irradiation. The characteristic green emission of the CPB QDs was observed. (**c**,**d**) Field-emission scanning electron microscopy (FE-SEM) images of CPB/SiO_2 NPs (**c**) and CPB-PPO/SiO_2 NPs (**d**).

The embedment of PPO molecules in the NPs was confirmed by FTIR spectroscopic measurements (Figure 2a). While any vibrational peak in the 1400–1600 cm^{-1} wavenumber region was absent for the CPB/SiO_2 NPs, the characteristic aromatic C=C vibrational peaks originated from the PPO molecules in that region were clearly observed in the spectrum of the CPB–PPO/SiO_2 NPs [15]. The encaging of the PPO molecules in the SiO_2 NPs also appeared to solve their problem of dispersibility in water. As shown in Figure 2b, the CPB–PPO/SiO_2 NPs were highly dispersible in water even at a high concentration of 10 mg/mL, but the unencapsulated PPO molecules were not soluble or dispersible in water. While the PPO molecules were precipitated in a short time, the dispersibility of the colloidal CPB–PPO/SiO_2 NPs in water was maintained for at least 1 h, as shown in Figure 2c. Not only the dispersibility of PPO molecules, but also their stability in SiO_2 NPs is important because of their potential for eye irritation and acute toxicity [16]. Electronic absorption measurements were performed to evaluate the stability of the embedded PPO molecules (Figure 2d,e). Prior to the evaluation, it was confirmed that the absorption intensity was almost exactly proportional to the PPO concentration, as shown in the inset of Figure 2d. Comparing these spectra, any detectable PPO signal was not observed for the solution, in which the CPB/SiO_2 NPs were dispersed for 30 days, indicating the high stability of

PPO molecules in the NPs. Furthermore, based on the report that most SiO_2 NPs of this size intravenously injected into mice are excreted within 7 days [9], the accumulated PPO or SiO_2 in the body would be much less. Of course, further in-depth evaluation will be required to safely apply this material to in vivo imaging.

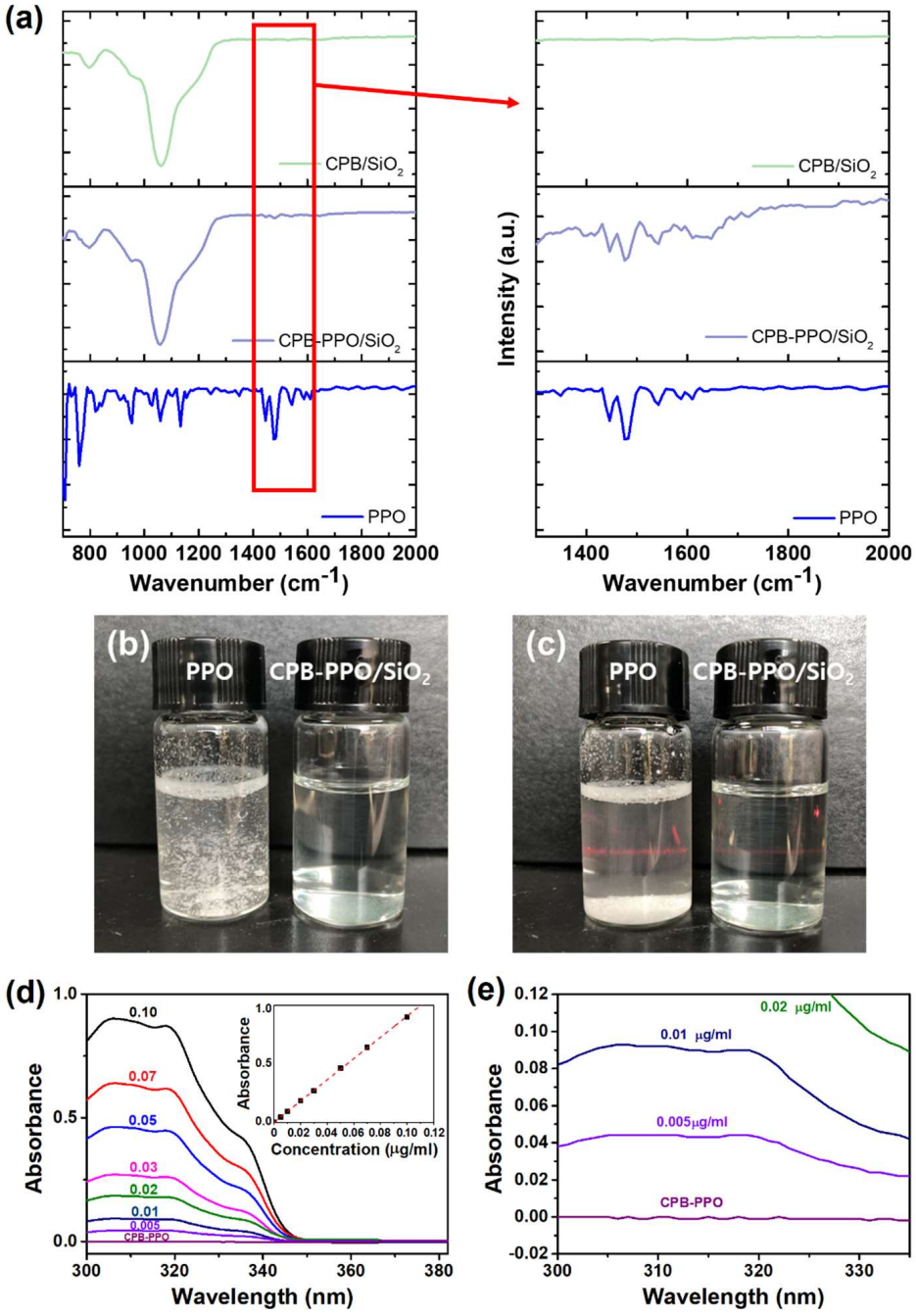

Figure 2. (**a**) Fourier-transform infrared (FTIR) spectra of CPB/SiO_2 NPs, CPB–PPO/SiO_2 NPs, and PPO molecules (from top to bottom). The magnified spectra over the wavenumber region of aromatic C=C vibration (1400–1600 cm^{-1}) are also shown on the right to confirm the embedment of PPO molecules in the CPB/SiO_2 NPs. (**b**,**c**) Photographs of PPO molecules and CPB–PPO/SiO_2 NPs dispersed in water, taken immediately (**b**) and 1 h after the dispersion (**c**). (**d**,**e**) Electronic absorption spectra of the solution containing CPB-PPO/SiO_2 NPs and solutions containing various concentrations of PPO in tolutene at the 300–380 nm (**d**) and 300–335 nm (**e**) wavelength region. The plot of absorbance vs. PPO concentration and the calibration curve are shown in the inset of (**d**).

As shown in Figure 3a–c, the addition of a small amount of PPO molecules in the CPB/SiO_2 NPs resulted in a brighter micro-CT image, which is attributed to the enhanced X-ray attenuation by the synergetic effect of the CPB QDs and PPO molecules (Figure 3a–c). The images were obtained under the same condition, i.e., a tube potential of 50 kVp and an NP concentration of 1.0 mg/mL. To more quantitatively investigate the enhancement of the X-ray attenuation quantum efficiency after the addition of PPO molecules in the CPB/SiO_2 NPs, the Hounsfield unit (HU) was calculated using the micro-CT imaging of the NP-dispersed aqueous solutions (Figure 3d). The HU is a quantitative measurement, which is proportional to the degree of X-ray attenuation when the X-ray penetrates the matter [17,18]. The corresponding HU value was calculated by the following equation:

$$\mathrm{HU} = \left(\frac{\mu_x - \mu_{water}}{\mu_{water} - \mu_{air}} \right) \times 1000 \quad (1)$$

where μ_x, μ_{water}, and μ_{air} are the attenuation coefficients of the sample solution, water, and air, respectively. Because the attenuation coefficient of the air is nearly zero, the change of one HU of the sample represents a change of the 0.1% attenuation coefficient with respect to that of water. The obtained HU of the CPB–PPO/SiO_2 NP solution was 154, which was significantly larger than that of the only-CPB-containing NP solution, i.e., 57.8. The brighter micro-CT image and the increased HU indicated that the X-ray attenuation capability of the CPB/SiO_2 NPs was effectively improved by the addition of PPO molecules.

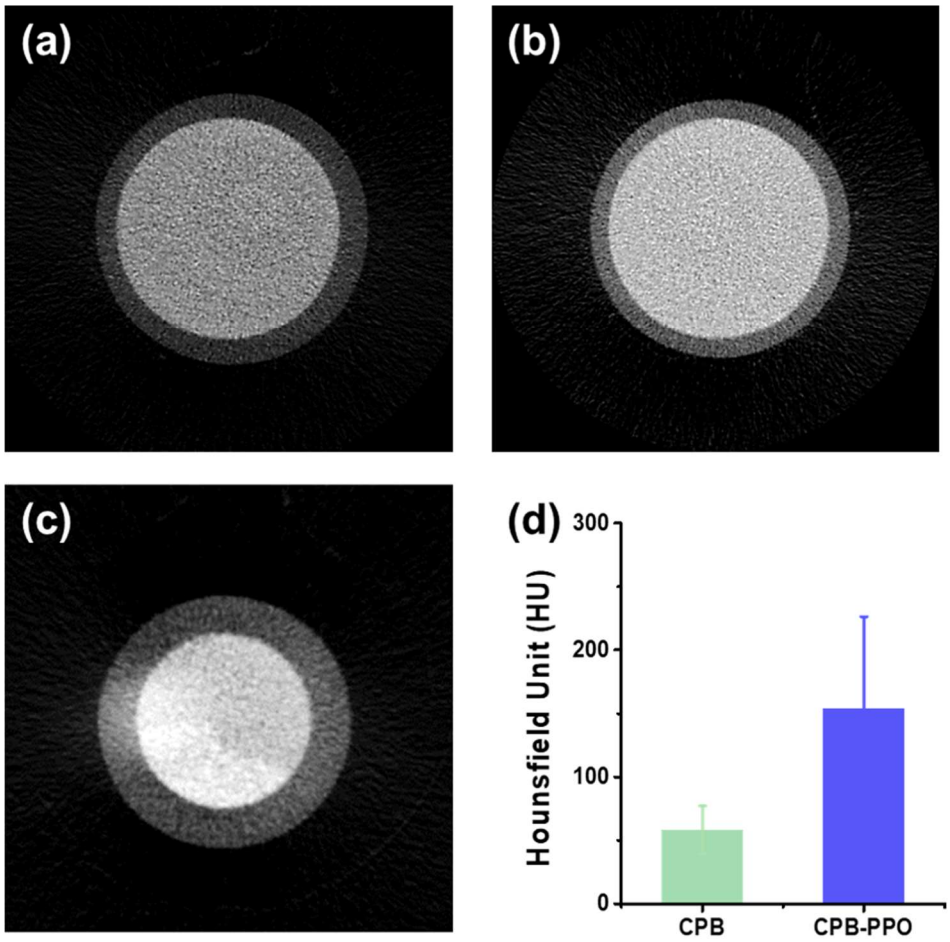

Figure 3. (**a**–**c**) Micro-computed tomography (CT) images of water (**a**), the CPB/SiO_2 NP solution (**b**), and the CPB–PPO/SiO_2 NP solution (**c**). The concentrations of both NP solutions were 1.0 mg/mL in water. (**d**) Hounsfield units of the CPB/SiO_2 and CPB–PPO/SiO_2 NP solutions.

4. Conclusions

In summary, we have developed a new synthetic route for X-ray-attenuating SiO_2 NPs, which contained CPB QDs and PPO molecules simultaneously. The synthesis was successfully achieved by rapidly mixing a CPB precursor solution containing a catalyst for SiO_2 synthesis and a SiO_2 precursor solution containing PPO molecules. The effective embedment of PPO molecules in SiO_2 NPs, confirmed by FTIR measurements, solved the poor dispersibility problem of organic PPO scintillators in water. The co-embedment of inorganic and organic scintillators in SiO_2 NPs resulted in a significant improvement in their X-ray-attenuating efficiencies. The HU of the 1.0 mg/mL CPB–PPO/SiO_2 NP solution was 154, which was approximately 2.7 times larger than that of the CPB/SiO_2 NP solution with the same concentration.

Author Contributions: S.Y. designed the study and wrote the manuscript. G.C. and H.K. performed the synthesis of quantum dots and nanoparticles. I.R. presented the idea and carried out HU measurements. All authors have read and agreed to the published version of the manuscript.

Funding: This research was funded by National Research Foundation of Korea (NRF; grant numbers: 2016R1A5A1012966, 2021R1A2C1009911, and 2021R1A6A3A01088245) funded by the Korean Government.

Data Availability Statement: The datasets generated during and/or analyzed during the current study are available from the corresponding author on reasonable request.

Conflicts of Interest: The authors declare no conflict of interest.

References

1. Michalet, X.; Pinaud, F.F.; Bentolila, L.A.; Tsay, J.M.; Doose, S.; Li, J.J.; Sundaresan, G.; Wu, A.M.; Gambhir, S.S.; Weiss, S. Quantum dots for live cells, in vivo imaging, and diagnostics. *Science* **2005**, *307*, 538–544. [CrossRef] [PubMed]
2. Smith, B.R.; Gambhir, S.S. Nanomaterials for In Vivo Imaging. *Chem. Rev.* **2017**, *117*, 901–986. [CrossRef] [PubMed]
3. Chen, G.; Roy, I.; Yang, C.; Prasad, P.N. Nanochemistry and Nanomedicine for Nanoparticle-based Diagnostics and Therapy. *Chem. Rev.* **2016**, *116*, 2826–2885. [CrossRef]
4. Weissleder, R.; Nahrendorf, M. Advancing biomedical imaging. *Proc. Natl. Acad. Sci. USA* **2015**, *112*, 14424–14428. [CrossRef] [PubMed]
5. Heinzmann, K.; Carter, L.M.; Lewis, J.S.; Aboagye, E.O. Multiplexed imaging for diagnosis and therapy. *Nat. Biomed. Eng.* **2017**, *1*, 697–713. [CrossRef]
6. McHugh, K.J.; Jing, L.; Behrens, A.M.; Jayawardena, S.; Tang, W.; Gao, M.; Langer, R.; Jaklenec, A. Biocompatible Semiconductor Quantum Dots as Cancer Imaging Agents. *Adv. Mater.* **2018**, *30*, 1706356. [CrossRef] [PubMed]
7. Dang, X.; Bardhan, N.M.; Qi, J.; Gu, L.; Eze, N.A.; Lin, C.-W.; Kataria, S.; Hammond, P.T.; Belcher, A.M. Deep-tissue optical imaging of near cellular-sized features. *Sci. Rep.* **2019**, *9*, 3873. [CrossRef] [PubMed]
8. Hillman, E.M.C.; Amoozegar, C.B.; Wang, T.; McCaslin, A.F.H.; Bouchard, M.B.; Mansfield, J.; Levenson, R.M. In vivo optical imaging and dynamic contrast methods for biomedical research. *Philos. Trans. R. Soc. A* **2011**, *369*, 4620–4643. [CrossRef]
9. Ryu, I.; Ryu, J.-Y.; Choe, G.; Kwon, H.; Park, H.; Cho, Y.-S.; Du, R.; Yim, S. In vivo plain X-ray imaging of cancer using perovskite quantum dot scintillators. *Adv. Funct. Mater.* **2021**, *31*, 2102334. [CrossRef]
10. Cho, S.; Kim, S.; Kim, J.; Jo, Y.; Ryu, I.; Hong, S.; Lee, J.-J.; Cha, S.; Nam, E.B.; Lee, S.U.; et al. Hybridisation of perovskite nanocrystals with organic molecules for highly efficient liquid scintillators. *Light Sci. Appl.* **2020**, *9*, 156. [CrossRef]
11. Adrova, N.A.; Koton, M.M.; Florinsky, F.S. Preparation of 2,5-diphenyloxazole and its scintillation efficiency in plastics. *Russ. Chem. Bull.* **1957**, *6*, 394–395. [CrossRef]
12. Maddalena, F.; Tjahjana, L.; Xie, A.; Arramel; Zeng, S.; Wang, H.; Coquet, P.; Drozdowski, W.; Dujardin, C.; Dang, C.; et al. Inorganic, Organic, and Perovskite Halides with Nanotechnology for igh-Light Yield X- and γ-ray Scintillators. *Crystals* **2019**, *9*, 88. [CrossRef]
13. Butkus, J.; Vashishtha, P.; Chen, K.; Gallaher, J.K.; Prasad, S.K.K.; Metin, D.Z.; Laufersky, G.; Gaston, N.; Halpert, J.E.; Hodgkiss, J.M. The Evolution of Quantum Confinement in $CsPbBr_3$ Perovskite Nanocrystals. *Chem. Mater.* **2017**, *29*, 3644–3652. [CrossRef]
14. Huang, H.; Polavarapu, L.; Sichert, J.A.; Susha, A.S.; Urban, A.S.; Rogach, A.L. Colloidal lead halide perovskite nanocrystals: Synthesis, optical properties and applications. *NPG Asia Mater.* **2016**, *8*, e328. [CrossRef]
15. Liu, Y.-L.; Chang, Y.-H.; Liang, M. Poly(2,6-dimethyl-1,4-phenylene oxide) (PPO) multi-bonded carbon nanotube (CNT): Preparation and formation of PPO/CNT nanocomposites. *Polymer* **2008**, *49*, 5405–5409. [CrossRef]
16. European Chemical Agency (ECHA). Available online: https://echa.europa.eu/information-on-chemicals/cl-inventory-database/-/discli/details/80386 (accessed on 19 November 2021).

17. DenOtter, T.D.; Schubert, J. *Hounsfield Unit*; StatPearls: Treasure Island, FL, USA, 2020. Available online: https://europepmc.org/article/nbk/nbk547721 (accessed on 8 December 2021).
18. Wendt, R. The Mathematics of Medical Imaging: A Beginner's Guide. *J. Nucl. Med.* **2010**, *51*, 1987. [CrossRef]